Journal of Scientific Computing (2019) 81:2115–2131
https://doi.org/10.1007/s10915-019-01073-3

Well-Balanced Discontinuous Galerkin Method for Shallow Water Equations with Constant Subtraction Techniques on Unstructured Meshes

Huijing Du[1] · Yingjie Liu[2] · Yuan Liu[3] · Zhiliang Xu[4]

Received: 22 February 2019 / Revised: 12 September 2019 / Accepted: 14 October 2019 /
Published online: 2 November 2019

Abstract
The classical Saint–Venant shallow water equations on complex geometries have wide applications in many areas including coastal engineering and atmospheric modeling. The main numerical challenge in simulating Saint–Venant equations is to maintain the high order of accuracy and well-balanced property simultaneously. In this paper, we propose a high-order accurate and well-balanced discontinuous Galerkin (DG) method on two dimensional (2D) unstructured meshes for the Saint–Venant shallow water equations. The technique used to maintain well-balanced property is called constant subtraction and proposed in Yang et al. (J Sci Comput 63:678–698, 2015). Hierarchical reconstruction limiter with a remainder correction technique is introduced to control numerical oscillations. Numerical examples with smooth and discontinuous solutions are provided to demonstrate the performance of our proposed DG methods.

Keywords Hyperbolic balance laws · Saint–Venant equations · Shallow water equations · Discontinuous Galerkin methods · Constant subtraction · Unstructured meshes · Hierarchical reconstruction · Remainder correction

1 Introduction

In this paper, we are interested in developing a high-order accurate and well-balanced discontinuous Galerkin (DG) method for solving the Saint–Venant shallow water equations on two dimensional (2D) unstructured meshes. The Saint–Venant shallow water equations consist of hyperbolic balance laws and take the following form [2]

Huijing Du: Research supported in part by NSF Grant DMS-1853636. Yingjie Liu: Research supported in part by NSF Grants DMS-1522585 and DMS-CDS & E-MSS-1622453. Yuan Liu: Research supported in part by a grant from the Simons Foundation (426993). Zhiliang Xu: Research supported in part by NSF Grants DMS-1517293, CDS& E-MSS-1821242 and CDS & E-MSS 1854779.

✉ Yuan Liu
liu@math.wichita.edu

Extended author information available on the last page of the article

$$\frac{\partial}{\partial t}\begin{bmatrix} h \\ h\mathbf{u} \end{bmatrix} + \nabla \cdot \begin{bmatrix} h\mathbf{u} \\ h\mathbf{u} \otimes \mathbf{u} + \frac{1}{2}gh^2\mathbb{I} \end{bmatrix} = \begin{bmatrix} 0 \\ -gh\nabla b \end{bmatrix}, \tag{1.1}$$

where h denotes the depth of water, $\mathbf{u} = (u, v)^T$ is the depth-averaged velocity, b describes the bottom topography, g is the gravitational constant, and $\otimes$ represents the tensor product of two vectors and $\mathbb{I}$ is the identity matrix.

While the shallow water equations with a non-flat bottom topography play a critical role in modeling flows in rivers, lakes and coastal areas [3,18,23,29], numerically solving this system of equations is challenging. One major numerical difficulty to simulate the shallow water Eq. (1.1) is due to the well-balanced property of (1.1), namely, system (1.1) admits all nontrivial equilibrium solutions given by

$$h + b \equiv \text{Constant}, \qquad \mathbf{u} \equiv \mathbf{0}. \tag{1.2}$$

The numerical methods, which preserve those steady states of 'a lake at rest' (1.2) at discrete level, are called well-balanced methods.

Many well-balanced numerical methods have been developed for solving shallow water equations. Our interests lie in high-order accurate numerical methods because they can achieve the desired resolution with less computational cost. Popular high-order well-balanced methods for shallow water equations include finite difference methods [20,30,32,33], finite volume methods [7–10,16,17,21,34] and finite element discontinuous Galerkin (DG) methods [34]. For a detailed overview of high-order well-balanced numerical methods, we refer readers to the review papers [22,31,36] and the references therein. Among various methods, DG methods are shown to have lots of advantages including high order of accuracy, flexibility for hp-adaptivity, parallel efficiency, and complex geometries. In the existing literature, several techniques have been developed within the DG framework in order to retain the well-balanced property. In [34], a special decomposition of the source term is used so that the resulted DG schemes are capable of maintaining the 'a lake at rest' steady state. Another popular approach is hydrostatic reconstruction [35,37]. With a modification of numerical flux, the DG schemes can maintain the well-balanced property and high order of accuracy simultaneously. The main advantage of this approach is its simple implementation and the additional computational cost is negligible compared with traditional DG. Path-conservative [25] is a third approach to construct well-balanced DG schemes. More recently, a constant subtraction technique was proposed in [40] to construct well-balanced finite volume schemes for shallow water system on structured meshes. By reformulating the system in terms of equilibrium variables, the well-balanced property is automatically achieved for general high-order finite volume schemes. Because of this attractive feature, in this paper, we further explore the potential of the constant subtraction technique [40] to construct a class of high-order well-balanced DG schemes on 2D unstructured meshes.

Besides the aforementioned numerical challenge caused by the well-balanced property, another standard difficulty of numerically solving nonlinear hyperbolic equations is to control oscillations in their numerical solutions. In particular, when the solutions contain strong discontinuities, limiting techniques are needed to ensure stability of the numerical simulation. Many limiting techniques have been developed over the past few decades including the total variation bounded (TVB) limiters [11–15,27], the moment limiters [4,6], weighted essentially non-oscillatory (WENO) methodology based limiters [24,41–45] and many others. Here, we will continue the research line on the development of hierarchical reconstruction (HR) limiting technique which are originally designed for hyperbolic conservation laws [38,39]. The main advantages of this limiting technique are that no local characteristic decomposition

is needed on structured or unstructured meshes and that significant spurious oscillations can be removed. In order to further control spurious oscillations in the numerical solutions while maintaining its high resolution near discontinuities, we generalize the remainder correction technique [40] and apply it to our DG solution in this paper.

The rest of this paper is organized as follows. In Sect. 2, we describe our proposed high-order accurate well-balanced DG scheme for the shallow water Eq. (1.1) on 2D unstructured meshes. In Sect. 3, we present the point-wise HR limiter with remainder correction technique. In Sect. 4, numerical simulations with smooth and discontinuous solutions are provided to demonstrate the effectiveness of our proposed DG method and limiting technique. Finally, concluding remarks are given in Sect. 5.

2 DG Framework on Triangular Meshes

In this section, we describe our proposed high-order well-balanced DG framework. The system (1.1) consists of the following component equations

$$\begin{cases} h_t + (hu)_x + (hv)_y = 0, \\ (hu)_t + (hu^2 + \frac{1}{2}gh^2)_x + (huv)_y = -ghb_x, \\ (hv)_t + (huv)_x + (hv^2 + \frac{1}{2}gh^2)_y = -ghb_y. \end{cases} \tag{2.1}$$

In order to achieve the well-balanced property, we firstly use the constant subtraction technique introduced in [40] to reformulate the shallow water equations.

We introduce some notations used throughout the paper. We denote the water surface as $w = h + b$, the equilibrium variables as $\mathbf{U} = (w, hu, hv)^T$ and the global spatial average of $w(x, y, t)$ on the entire computational domain Ω as

$$\bar{w}(t) = \frac{1}{|\Omega|}\int_{\Omega} w(x, y, t)d\Omega. \tag{2.2}$$

Using $\bar{w}$, the right hand side terms in (2.1) can be decomposed as

$$-ghb_x = \left(\frac{1}{2}gb^2\right)_x + (-g\bar{w}b)_x + g(\bar{w} - w)b_x, \tag{2.3}$$

$$-ghb_y = \left(\frac{1}{2}gb^2\right)_y + (-g\bar{w}b)_y + g(\bar{w} - w)b_y. \tag{2.4}$$

Then, the shallow water Eq. (2.1) can be reformulated in terms of the equilibrium variables,

$$\mathbf{U}_t + \nabla \cdot \mathbf{F}(\mathbf{U}) = \mathbf{S}(\mathbf{U}, b, t), \tag{2.5}$$

where

$$\mathbf{U} = \begin{bmatrix} w \\ hu \\ hv \end{bmatrix}, \mathbf{F}(\mathbf{U}) = [F_1(\mathbf{U}), \quad F_2(\mathbf{U})], \qquad \mathbf{S}(\mathbf{U}, b, t) = \begin{bmatrix} 0 \\ g(\bar{w} - w)b_x \\ g(\bar{w} - w)b_y \end{bmatrix}, \tag{2.6}$$

and

$$F_1(\mathbf{U}) = \begin{bmatrix} hu \\ \frac{(hu)^2}{w-b} + g(\bar{w} - w)b + \frac{g}{2}w^2 \\ \frac{(hu)(hv)}{w-b} \end{bmatrix}, \qquad F_2(\mathbf{U}) = \begin{bmatrix} hv \\ \frac{(hu)(hv)}{w-b} \\ \frac{(hv)^2}{w-b} + g(\bar{w} - w)b + \frac{g}{2}w^2 \end{bmatrix}. \tag{2.7}$$

It can be verified that the system (2.5)–(2.7) is equivalent to (2.1) for both smooth and nonsmooth solutions, and the terms $g(\bar{w}-w)b_x$, $g(\bar{w}-w)b_y$ will automatically vanish at 'a lake at rest' steady states.

We propose to solve the system (2.5)–(2.7) by a Runge–Kutta discontinuous Galerkin (RKDG) method. Let $\Omega = \cup_{i=1}^{N}\Omega_i$ be a shape-regular triangular partition of the 2D computational domain, and denote the numerical approximation of $\mathbf{U}$ as $\mathbf{U}_h$. The DG method to solve (2.5) -(2.7) is defined by: find the numerical approximation $\mathbf{U}_h$ in the finite element space V_Ω^k

$$V_\Omega^k = \{\mathbf{v}_h \in [L^2(\Omega)]^3 : \quad \mathbf{v}_h|_{\Omega_i} \in [P^k(\Omega_i)]^3, i = 1, 2, \dots N\}, \tag{2.8}$$

where $P^k(\Omega_i)$ denotes the space of polynomials on Ω_i of degree at most k, such that

$$\frac{d}{dt}\int_{\Omega_i}\mathbf{U}_h\cdot\mathbf{v}_h d\mathbf{x} + \int_{\partial\Omega_i}\hat{\mathbf{F}}\cdot\mathbf{n}_i\cdot\mathbf{v}_h ds - \int_{\Omega_i}\left(F_1\cdot\frac{\partial\mathbf{v}_h}{\partial x} + F_2\cdot\frac{\partial\mathbf{v}_h}{\partial y}\right)d\mathbf{x} = \int_{\Omega_i}\mathbf{S}\cdot\mathbf{v}_h d\mathbf{x}. \tag{2.9}$$

Here, $\mathbf{v}_h(\mathbf{x})$ is any test function from the space V_Ω^k and $\mathbf{n}_i$ is the unit outward-pointing normal vector on the boundary of cell Ω_i. $\hat{\mathbf{F}}$ is the so called numerical flux which is defined as

$$\hat{\mathbf{F}}\cdot\mathbf{n}_i = \mathcal{F}(\mathbf{U}_h^{in}, \mathbf{U}_h^{out}, \mathbf{n}_i) \tag{2.10}$$

where $\mathbf{U}_h^{in}$ and $\mathbf{U}_h^{out}$ are traces of the numerical solutions $\mathbf{U}_h$ on the boundary $\partial\Omega_i$ obtained from the interior and exterior of Ω_i. In this paper, we choose to employ the local Lax–Friedrichs flux in the numerical implementation, i.e. $\mathcal{F}$ is given as

$$\mathcal{F}(\mathbf{a},\mathbf{b},\mathbf{n}_i) = \frac{1}{2}(\mathbf{F}(\mathbf{a})\cdot\mathbf{n}_i + \mathbf{F}(\mathbf{b})\cdot\mathbf{n}_i - \alpha(\mathbf{b}-\mathbf{a})), \tag{2.11}$$

$$\alpha = \max((|u| + \sqrt{gh}, |v| + \sqrt{gh})\cdot\mathbf{n}_i), \tag{2.12}$$

where the maximum is taken over the neighborhood of the control volume.

The semi-discrete ODE systems (2.9) can then be evolved by a s-stage TVD Runge–Kutta method. In our numerical simulation, we employ the second-order and third-order TVD Runge–Kutta methods [28] which take the following forms:

$$\begin{aligned} U^{(1)} &= U^n + \Delta t\mathscr{L}(U^n),\\ U^{n+1} &= \frac{1}{2}U^n + \frac{1}{2}U^{(1)} + \frac{1}{2}\Delta t\mathscr{L}(U^{(1)}); \end{aligned} \tag{2.13}$$

and

$$\begin{aligned} U^{(1)} &= U^n + \Delta t\mathscr{L}(U^n),\\ U^{(2)} &= \frac{3}{4}U^n + \frac{1}{4}U^{(1)} + \frac{1}{4}\Delta t\mathscr{L}(U^{(1)}),\\ U^{n+1} &= \frac{1}{3}U^n + \frac{2}{3}U^{(2)} + \frac{2}{3}\Delta t\mathscr{L}(U^{(2)}). \end{aligned} \tag{2.14}$$

Here $\mathscr{L}$ is the spatial operator when representing (2.9) as $\frac{dU}{dt} = \mathscr{L}(U)$.

Theorem 1 *The semi-discrete DG scheme* (2.9) *with TVD Runge–Kutta methods for system* (2.5)–(2.7) *preserves the well-balanced property.*

Proof Assume that the numerical solutions of system (2.5)–(2.7) at $t = t^n$ are at 'a lake at rest' steady state, i.e.,

$$w^n = \text{const} \qquad (hu)^n = (hv)^n = 0. \tag{2.15}$$

It indicates that the DG approximations at $t = t^n$ are all constant polynomials. Therefore, the high-order DG reconstruction process for the equilibrium variables $(w, hu, hv)^T$ are also the same constants. When $u_h^{in} = u_h^{out}$, the numerical flux $\hat{\mathbf{F}}$ is consistent with the physical flux $\mathbf{F}$ at the cell interfaces, i.e., $\hat{\mathbf{F}}|_{\partial\Omega_i} = \mathbf{F}|_{\partial\Omega_i}$. Furthermore, by the divergence theorem, we have

$$\begin{aligned} \int_{\partial\Omega_i} \hat{\mathbf{F}} \cdot \mathbf{n}_i \cdot \mathbf{v}_h ds &= \int_{\partial\Omega_i} \mathbf{F} \cdot \mathbf{n}_i \cdot \mathbf{v}_h ds \\ &= \int_{\Omega_i} \mathbf{F} \cdot \nabla \mathbf{v}_h d\mathbf{x} \\ &= \int_{\Omega_i} \left(F_1 \cdot \frac{\partial \mathbf{v}_h}{\partial x} + F_2 \cdot \frac{\partial \mathbf{v}_h}{\partial y} \right) d\mathbf{x} \end{aligned} \tag{2.16}$$

On the other hand, the reconstructed DG polynomial for w is the same as $\bar{w}$ and the source terms in (2.9) vanish. We then have

$$\frac{d}{dt} \int_{\Omega_i} \mathbf{U}_h \cdot \mathbf{v}_h d\mathbf{x} = 0. \tag{2.17}$$

We then conclude that the DG approximation at $t = t^{n+1}$ also satisfies $w^{n+1} = \text{const}$ and $(hu)^{n+1} = (hv)^{n+1} = 0$ with any TVD Runge–Kutta methods, i.e. the well-balanced property is preserved. □

3 Point-Wise Hierarchical Reconstruction (HR)

In this section, we present our HR techniques employed in limiting the DG solution on 2D unstructured meshes. We first give a synopsis of the main idea of HR limiting. Let Ω_I be the control volume and the set $\{\Omega_j\}_{j\in J}$ be the collection of cells adjacent to Ω_I. We denote $\mathbf{x}_j$, $j \in \{I, J\}$ as the cell centroids of cells Ω_I and $\{\Omega_j\}_{j\in J}$ respectively. For a DG scheme at each time step, we will have the polynomial approximations, which can be reformulated as the following form of Taylor series expansion

$$u_j(\mathbf{x} - \mathbf{x}_j) = \sum_{m=0}^{d} \sum_{|\mathbf{m}|} \frac{1}{\mathbf{m}!} u_j^{\mathbf{m}}(\mathbf{x}_j)(\mathbf{x} - \mathbf{x}_j)^{\mathbf{m}}, \quad j \in \{I, J\}, \tag{3.1}$$

where d is the degree of the polynomials of numerical approximations.

The general procedure of point-wise HR is to modify the numerical solution polynomials $u_j(\mathbf{x}-\mathbf{x}_j)$ to non-oscillatory polynomials $\tilde{u}_j(\mathbf{x}-\mathbf{x}_j)$ with the same order of accuracy. To this end, we need to reconstruct coefficients $u_j^{\mathbf{m}}(\mathbf{x}_j)$ to obtain a new set of coefficients $\tilde{u}_j^{\mathbf{m}}(\mathbf{x}_j)$. The detailed implementation procedure is summarized in the following:

Point-Wise HR Algorithm

Step 1. Suppose $d \geq 2$. For $m = d, d-1, \ldots, 1$, do the following:

(a) Take the $(m-1)$th order partial derivative of $\{u_j(\mathbf{x}-\mathbf{x}_j)\}_{j=I,J}$ and write $\partial^{(m-1)}u_I(\mathbf{x}-\mathbf{x}_I) = L_{m,I}(\mathbf{x}-\mathbf{x}_I)+R_{m,I}(\mathbf{x}-\mathbf{x}_I)$, where $L_{m,I}(\mathbf{x}-\mathbf{x}_I)$ is the linear part and $R_{m,I}(\mathbf{x}-\mathbf{x}_I)$ is the remainder.
(b) Compute the cell average of $\partial^{(m-1)}u_I(\mathbf{x}-\mathbf{x}_I)$ over cell Ω_I to obtain $\overline{\partial^{(m-1)}u_I}$. Calculate the point-average of $\partial^{(m-1)}u_j(\mathbf{x}-\mathbf{x}_j)$ over cell Ω_j to obtain $\overline{\partial^{(m-1)}u_j}$, $j \in J$. (Here, the point-average is defined in Remark 1.)
(c) Let $\widetilde{R}_{m,I}(\mathbf{x}-\mathbf{x}_I)$ denote $R_{m,I}(\mathbf{x}-\mathbf{x}_I)$ with its coefficients replaced by the corresponding modified values. The remainder $R_{m,I}(\mathbf{x}-\mathbf{x}_I)$ of this step consists the 2nd or higher-order terms of the polynomial $\partial^{(m-1)}u_I(\mathbf{x}-\mathbf{x}_I)$, and the coefficients of the remainder are already reconstructed in the previous HR iterative steps. Here after the coefficients of $R_{m,I}(\mathbf{x}-\mathbf{x}_I)$ are replaced by their reconstructed new values, $R_{m,I}(\mathbf{x}-\mathbf{x}_i)$ becomes $\widetilde{R}_{m,I}(\mathbf{x}-\mathbf{x}_I)$.) Compute the cell average of $\widetilde{R}_{m,I}(\mathbf{x}-\mathbf{x}_I)$ on cell Ω_I to obtain $\overline{\widetilde{R}_{m,I}}$. Compute the point-average of $\widetilde{R}_{m,j}(\mathbf{x}-\mathbf{x}_j)$ on cell Ω_j to obtain $\overline{\widetilde{R}_{m,j}}$, $j \in J$.
(d) Let $\overline{L}_{m,j} = \overline{\partial^{(m-1)}u_j} - \overline{\widetilde{R}_{m,j}}$ for cell Ω_j, $j \in \{I, J\}$.
(e) Using $\{\overline{L}_{m,j}\}_{j\in\{I,J\}}$ to reconstruct $L_{m,I}$ on Ω_I by a weighted combination such that $L_{m,I}$ is non-oscillatory.
(f) Repeat from (a) to (e) until all possible combinations of the $(m-1)$th order partial derivatives are taken.

Step 2. The new 0th order coefficient of $u_I(\mathbf{x}-\mathbf{x}_I)$ is chosen such that the cell average of $\widetilde{u}_I(\mathbf{x}-\mathbf{x}_I)$ is equal to the cell average of $u_I(\mathbf{x}-\mathbf{x}_I)$ on cell Ω_I.

Remark 1 We define the average of a set of point-wise values of a polynomial v_h over a cell Ω_j to be the point-average, which is computed by $\left(\sum_{k=1}^{N} v_h(\mathbf{x}_{k,j})\right)/N$, where $\{\mathbf{x}_{k,j} : k = 1, \ldots, N\}$ is a set of points in cell Ω_j, where the points are chosen in the same way as in [38].

It is proved in [38] that, under certain requirements of the distribution of the stencil centroids, the point-wise HR limiting technique retains the approximation order of accuracy of the original polynomials. However, as any of the existing high-order limiting techniques, the HR is capable of limiting the spurious oscillations, which unfortunately cannot be completely eliminated, especially in the most demanding shallow water equations containing nonconservative source terms appearing on the right hand side of (1.1) in the case of discontinuous bottom topography function b. In this sense, we follow the work [40] and introduce the remainder correction technique to further regulate the remainder term $\widetilde{R}_{m,I}(\mathbf{x}-\mathbf{x}_I)$ in Step 1(c) of **Point-wise HR Algorithm**. This technique does not affect its approximation order of accuracy and further reduces possible overshoots/undershoots near discontinuities.

Here, we present the remainder correction technique used for the third-order HR limiting, i.e. in the case of $d = 2$. Let

$$\widetilde{R}_{m,I}(\mathbf{x}-\mathbf{x}_I) = a_1(x-x_I)^2 + a_2(x-x_I)(y-y_I) + a_3(y-y_I)^2. \tag{3.2}$$

Obviously, $\widetilde{R}_{m,I}(\mathbf{x}-\mathbf{x}_I) = \mathcal{O}\left((\Delta h)^2\right)$ in Ω_I, where Δh is the spatial mesh size. We propose to modify the remainder polynomial as

$$\widetilde{\widetilde{R}}_{m,I} = \frac{\widetilde{R}_{m,I}}{1 + |a_1|(x-x_I)^2 + |a_2||(x-x_I)(y-y_I)| + |a_3|(y-y_I)^2}. \tag{3.3}$$

In the following theorem, we show that the corrected remainder $\widetilde{\widetilde{R}}_{m,I}$ satisfies the following two conditions:

$$\begin{cases} \widetilde{\widetilde{R}}_{m,I}(\mathbf{x}-\mathbf{x}_I) = \widetilde{R}_{m,I}(\mathbf{x}-\mathbf{x}_I) + \mathcal{O}\left((\Delta h)^3\right), \quad \forall \mathbf{x} \in \Omega_I, \\ |\widetilde{\widetilde{R}}_{m,I}| < M, \quad \forall \mathbf{x} \in \mathbb{R}^2, \quad \text{for some constant } M. \end{cases} \tag{3.4}$$

Theorem 2 *The corrected remainder $\widetilde{\widetilde{R}}_{m,I}$ given by (3.3) satisfies the two conditions in (3.4).*

Proof The definition of $\widetilde{\widetilde{R}}_{m,I}$ in (3.3) and the fact that $\widetilde{R}_{m,I}(\mathbf{x}-\mathbf{x}_I) = \mathcal{O}\left((\Delta h)^2\right)$ in Ω_I imply that the first condition in (3.4) holds, namely:

$$\begin{aligned} \widetilde{\widetilde{R}}_{m,I} &= \widetilde{R}_{m,I}\left[1 + \mathcal{O}\left(|a_1|(x-x_I)^2 + |a_2||(x-x_I)(y-y_I)| + |a_3|(y-y_I)^2\right)\right] \\ &= \widetilde{R}_{m,I}\left[1 + \mathcal{O}\left((\Delta h)^2\right)\right] \\ &= \widetilde{R}_{m,I} + \mathcal{O}\left((\Delta h)^4\right), \forall \mathbf{x} \in \Omega_I. \end{aligned}$$

The second condition in (3.4) holds because $\widetilde{\widetilde{R}}_{m,I}$ is continuous and

$$\lim_{|\mathbf{x}|\to\infty} \left|\widetilde{\widetilde{R}}_{m,I}\right| = \lim_{|\mathbf{x}|\to\infty} \left| \frac{a_1(x-x_I)^2 + a_2(x-x_I)(y-y_I) + a_3(y-y_I)^2}{1 + |a_1|(x-x_I)^2 + |a_2||(x-x_I)(y-y_I)| + |a_3|(y-y_I)^2} \right| \leq 1$$

□

Remark 2 The remainder polynomial $\widetilde{\widetilde{R}}_{m,I}$ in (3.3) can also be taken as

$$\widetilde{\widetilde{R}}_{m,I} = \frac{\widetilde{R}_{m,I}}{1 + \gamma l(x,y) + q(x,y)} \tag{3.5}$$

with $l(x,y) = |c_1(x-x_I)| + |c_2(y-y_I)|$ and $q(x,y) = |a_1|(x-x_I)^2 + |a_2||(x-x_I)(y-y_I)| + |a_3|(y-y_I)^2$. Here, $c_1(x-x_I) + c_2(y-y_I)$ is the corresponding first order terms in $L_{m,I}(\mathbf{x}-\mathbf{x}_I)$ after the DG approximation, and $\gamma \geq 0$. Similar as in Theorem 2, it can be proved that (3.5) holds for the two conditions in (3.4).

Because of the first condition in (3.4), our proposed remainder correction technique will maintain the original high order of accuracy. The second condition in (3.4) is introduced to control the spurious oscillations, because $\widetilde{R}_{m,I}(\mathbf{x}-\mathbf{x}_I)$ grows quite fast away from $\mathbf{x}_I$ and the values $\widetilde{R}_{m,j}(\mathbf{x}-\mathbf{x}_j)$ used in Step 1(d) of **Point-wise HR Algorithm** may lead to oscillations. Therefore, we conclude that our proposed remainder correction technique can further reduce the oscillation while maintaining the original order of accuracy at the same time.

4 Numerical Examples

In this section, we present numerical results of our proposed well-balanced DG methods when applied to solve shallow water equations with various initial and boundary conditions on 2D unstructured meshes. Second order TVD Runge–Kutta time integrator is used when P^1 polynomial space is used for DG discretization, while third order TVD Runge–Kutta time integrator is used for P^2 case. Local Lax–Friedrichs numerical flux is used in all the examples and the gravitation acceleration constant g is fixed as 9.812 m/s^2. The CFL number is taken as 0.1 unless otherwise specified.

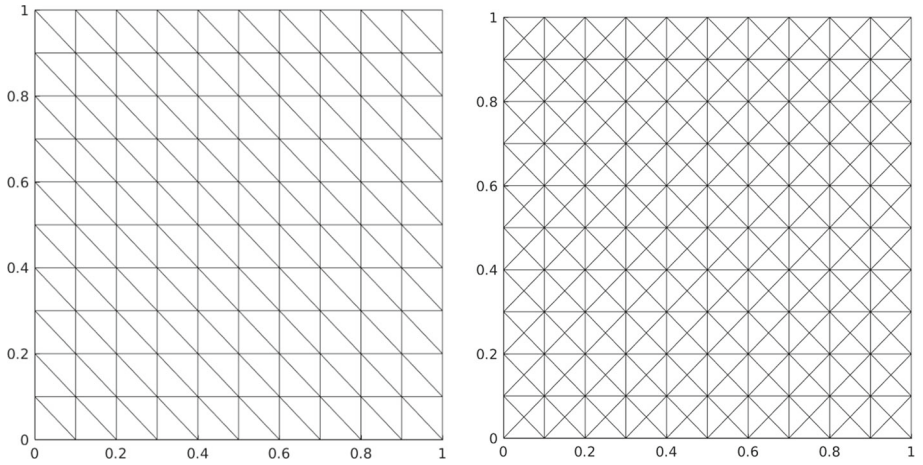

Fig. 1 The computational domain and sample triangular meshes of the numerical examples in Sect. 4. Left: with mesh size $\Delta h = 0.1$ for Examples 1 and 2; Right: with mesh size $\Delta h = 0.1$ for Example 3

Example 1 (*Verification of well-balanced property*) We verify the well-balanced property of our proposed method towards the steady-state solution in this example. This test problem is taken from [37]. On the rectangular computational domain $[0, 1] \times [0, 1]$, the bottom function is taken as

$$b(x, y) = \max(0, 1 - (10x - 5)^2 - (10y - 5)^2),$$

and the initial data is the "lake at rest" stationary solution:

$$\begin{aligned} w(x, y, 0) &= 2, \\ (hu)(x, y, 0) &= (hv)(x, y, 0) = 0. \end{aligned}$$

Periodic boundary conditions are used here. With this setup, it is desired that the steady state solutions are exactly preserved and the surface remains flat. We solve the shallow water system with our proposed DG schemes on the triangular meshes shown in the left panel of Fig. 1. Numerical solutions with different mesh sizes Δh are computed at time $T = 0.5$ with double-precision. In Table 1, we present the L^1 and L^∞-errors of the surface level w and discharges hu and hv computed by P^1 and P^2 DG schemes. We can clearly observe that all the numerical quantities are machine zeros, which numerically confirms that our proposed DG schemes preserve well-balanced property. We then test the effect of HR limiting techniques and the numerical errors are given in Table 2. All the numerical errors remain at the level of round-off errors which indicates that the DG schemes with HR limiting technique still hold well-balanced property.

Example 2 (*Accuracy test*) In this example, we will perform the accuracy test of our proposed method. Consider the shallow water equations on two dimensional computational domain $[0, 1] \times [0, 1]$. The bottom topography is

$$b(x, y) = \sin(2\pi x) + \cos(2\pi y),$$

Table 1 Example 1: L^1 and L^∞-errors for the stationary solution computed by well-balanced DG schemes only. Final time $T = 0.5$

Δh	L^1-error			L^∞-error		
	w	hu	hv	w	hu	hv
P^1 case						
1/10	4.07E−15	1.44E−14	1.31E−14	8.44E−15	4.77E−14	4.60E−14
1/20	9.04E−15	3.64E−14	3.82E−14	1.58E−14	1.27E−13	1.39E−13
1/40	2.10E−14	9.25E−14	9.31E−14	3.84E−14	3.70E−13	3.78E−13
1/80	3.92E−14	2.63E−13	2.62E−13	7.97E−14	1.54E−12	1.41E−12
1/160	7.45E−14	6.94E−13	6.92E−13	1.82E−13	4.02E−12	4.38E−12
P^2 case						
1/10	4.25E−14	7.06E−14	7.21E−14	5.28E−14	2.34E−13	2.09E−13
1/20	8.89E−14	1.36E−13	1.37E−13	1.12E−13	6.66E−13	5.48E−13
1/40	1.81E−13	2.68E−13	2.66E−13	2.17E−13	1.29E−12	1.30E−12
1/80	3.67E−13	5.33E−13	5.35E−13	4.58E−13	2.97E−12	3.51E−12
1/160	7.44E−13	1.05E−12	1.05E−12	9.38E−13	6.74E−12	8.82E−12

Table 2 Example 1: L^1 and L^∞-errors for the stationary solution computed by well-balanced DG schemes with HR limiting techniques. Final time $T = 0.5$

Δh	L^1-error			L^∞-error		
	w	hu	hv	w	hu	hv
P^1 case						
1/10	6.07E−17	8.14E−16	1.88E−15	1.11E−15	4.56E−15	7.26E−15
1/20	6.06E−17	9.73E−16	1.61E−15	1.11E−15	9.92E−15	6.95E−15
1/40	6.92E−17	1.08E−15	2.74E−15	1.11E−15	9.78E−15	1.81E−14
1/80	6.43E−17	9.52E−16	2.74E−15	1.11E−15	1.14E−14	3.76E−14
1/160	6.54E−17	9.45E−16	3.17E−15	1.11E−15	1.52E−14	3.70E−14
P^2 case						
1/10	1.88E−14	1.22E−14	9.69E−15	2.33E−14	5.37E−14	3.52E−14
1/20	5.47E−14	1.65E−14	1.72E−14	6.31E−14	1.14E−13	1.00E−13
1/40	1.31E−13	3.50E−14	3.81E−14	1.49E−13	2.05E−13	2.19E−13
1/80	2.98E−13	7.95E−14	8.06E−14	3.20E−13	6.32E−13	1.04E−12
1/160	6.58E−13	1.81E−13	1.80E−13	7.10E−13	2.32E−12	1.95E−12

and the initial data are given by

$$\begin{aligned} h(x, y, 0) &= 10 + e^{\sin(2\pi x)} \cos(2\pi y), \\ (hu)(x, y, 0) &= \sin(\cos(2\pi x)) \sin(2\pi y), \\ (hv)(x, y, 0) &= \cos(2\pi x) \cos(\sin(2\pi y)). \end{aligned}$$

The periodic boundary conditions are applied. The final time is taken as $T = 0.05$ to avoid the appearance of shocks in the solution. Since the exact solution is not available explicitly,

Table 3 Example 2: L^1 and L^∞ numerical orders computed by DG schemes at time $T = 0.05$

Δh	L^1 error order			L^∞ error order		
	w	hu	hv	w	hu	hv
P^1 case						
1/40	1.83	2.08	1.85	1.34	1.78	1.55
1/80	2.16	1.94	2.14	1.53	1.73	0.97
1/160	2.05	1.80	1.88	2.31	1.45	2.71
1/320	1.64	1.89	1.77	1.87	2.15	1.40
P^2 case						
1/40	2.01	2.38	2.07	1.06	1.71	1.10
1/80	2.82	2.36	2.70	1.50	1.34	1.68
1/160	3.53	2.69	3.52	4.75	3.86	4.64
1/320	3.39	2.42	3.06	2.43	2.38	3.59

Table 4 Example 2: L^1 and L^∞ numerical orders computed by DG schemes with HR limiting techniques at time $T = 0.05$

Δh	L^1 error order			L^∞ error order		
	w	hu	hv	w	hu	hv
P^1 case						
1/40	1.64	1.47	1.71	1.33	1.07	1.10
1/80	2.12	2.23	2.16	1.13	2.10	0.61
1/160	2.37	2.49	2.30	2.44	2.14	2.84
1/320	2.24	2.46	2.33	2.16	2.28	2.29
P^2 case						
1/40	2.12	2.93	2.14	1.35	2.45	1.36
1/80	2.41	2.93	2.47	2.01	2.34	2.15
1/160	2.87	2.99	2.91	2.50	2.89	2.74
1/320	3.01	2.94	2.96	2.60	2.80	2.62

we calculate the experimental order r by Aitken's formula [1], i.e.,

$$r = \log_2 \left(\frac{||u_{\frac{\Delta h}{2}} - u_{\Delta h}||}{||u_{\frac{\Delta h}{4}} - u_{\frac{\Delta h}{2}}||} \right),$$

where $u_{\Delta h}$ denotes the numerical solution computed using the triangular meshes of size Δh. The computational domain, and a sample triangular mesh with $\Delta h = 0.1$ are shown in the left panel of Fig. 1.

Table 3 contains the experimental orders of accuracy in the L^1 and L^∞-errors. As one can clearly see, the expected second and third order of accuracy are attained for both surface level w and discharges hu and hv. Furthermore, we perform the numerical simulation with DG schemes with HR limiting techniques. The numerical results are present in Table 4, in which we can still observe second and third order of accuracy. This results verifies that our HR limiting techniques do not affect the original high order of accuracy.

Example 3 (*Water drop problem*) Next, our methods are applied to a numerical test case which simulates the water drop problem. Following the setup in [26,37], we consider the 2D

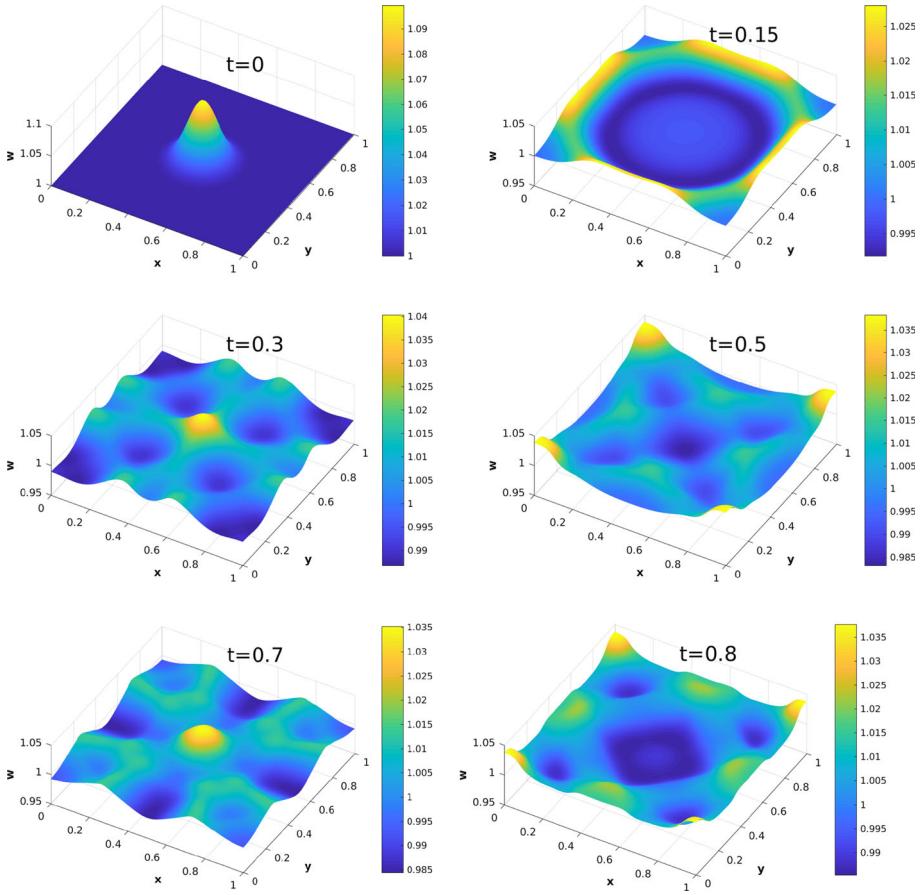

Fig. 2 Example 3: the water surface level with the flat bottom topography at different times

Gaussian shaped peak initial condition given by:

$$h(x, y, 0) = 1 + 0.1 \exp\left(-100\left((x-0.5)^2 + (y-0.5)^2\right)\right),$$
$$(hu)(x, y, 0) = (hv)(x, y, 0) = 0,$$

in the computational domain $[0, 1] \times [0, 1]$ with zero bottom topography. The reflective boundary conditions are employed. The initial Gaussian shaped water drop generates a wave that reflects off the boundary. The triangular mesh with $\Delta h = 1/80$ is generated as in the right panel of Fig. 1. We have provided the evolution of water surface at various times in Fig. 2, which shows that the wave is well simulated by our methods.

As a comparison, we also repeat the test with a non-zero bottom topography:

$$b(x, y) = 0.5 \exp\left(-10\left((x-0.75)^2 + (y-0.75)^2\right)\right). \tag{4.1}$$

The results are shown in Fig. 3.

Example 4 (*Small perturbation problem*) This is a classical example to show the capability of the proposed scheme for the perturbation of the stationary state. This test was given by LeVeque [19], and has also been used in [5,32,35,37].

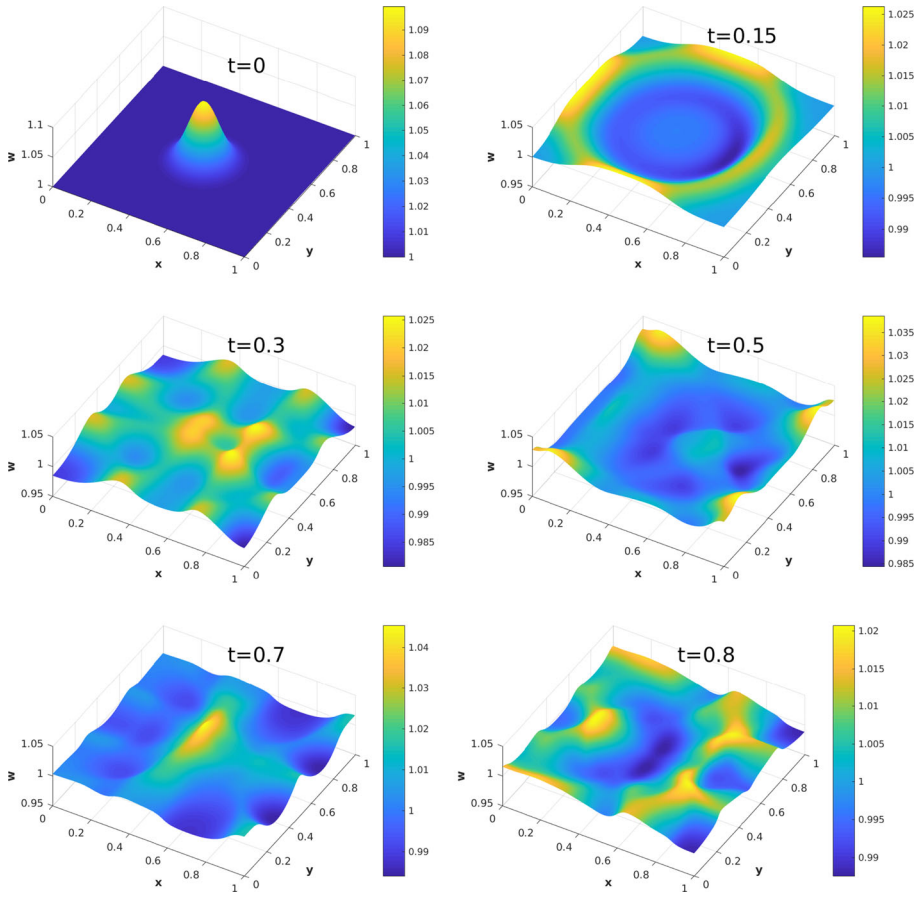

Fig. 3 Example 3: the water surface level with the bottom topography (4.1) at different times

The computational domain is $[0, 2] \times [0, 1]$. The bottom topography is an isolated elliptical-shaped hump:

$$b(x, y) = 0.8 \exp\left(-5\,(x - 0.9)^2 - 50\,(y - 0.5)^2\right).$$

The initial condition is given by

$$w(x, y, 0) = \begin{cases} 1 + 0.0001, & \text{if } 0.05 \le x \le 0.15, \\ 1, & \text{otherwise,} \end{cases}$$
$$(hu)(x, y, 0) = (hv)(x, y, 0) = 0.$$

The outlet boundary conditions are imposed on the left and right sides, and the reflective boundary conditions on the top and bottom sides.

Initially, the surface level is almost flat except for $0.05 \le x \le 0.15$, where w is perturbed upward by a small magnitude of 0.0001, which will split into two waves, propagating left and right at the characteristic speeds $\pm\sqrt{g(w - b)}$. The left-going disturbance wave leaves the domain and does not affect the solution after this. We compute the solution and monitor

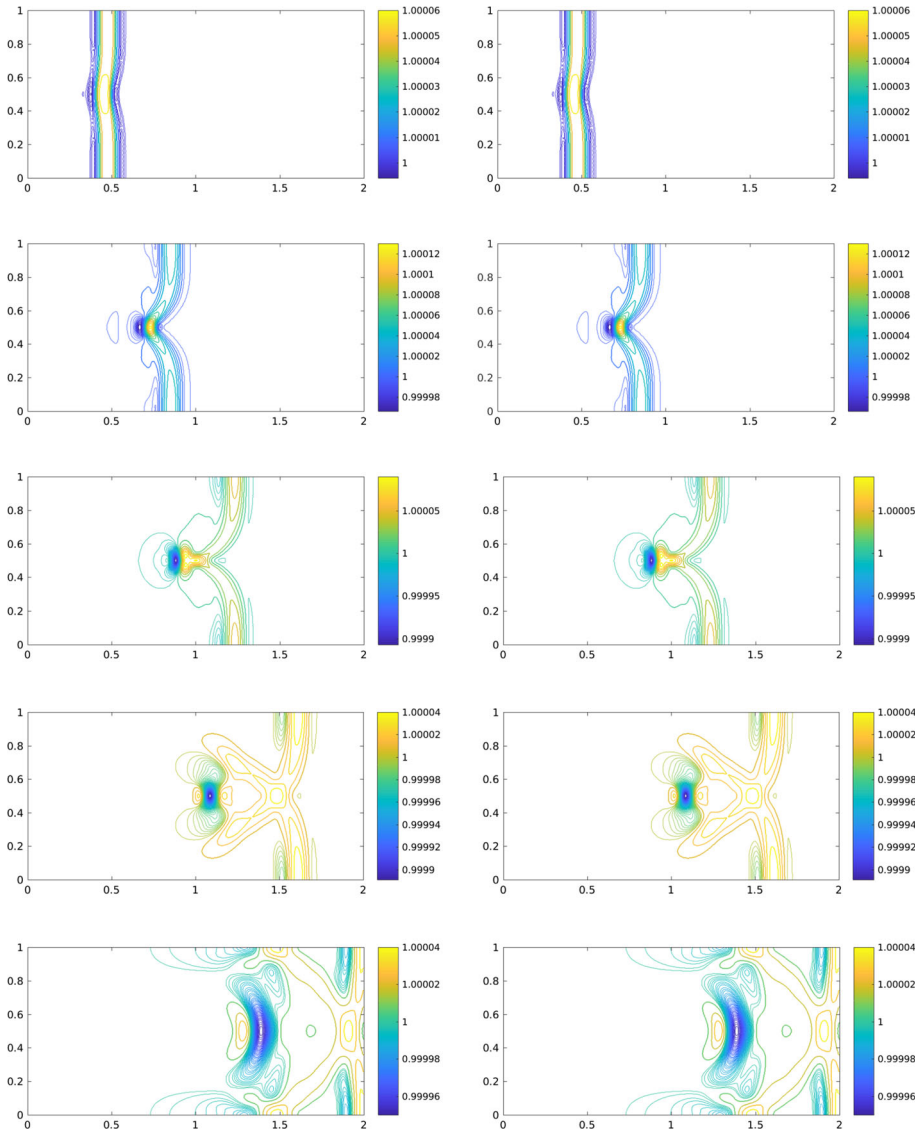

Fig. 4 Example 4: contour plot of water surface level w on 80×40 (left) and 320×160 (right) triangular meshes. The solution is shown at times $t = 0.12, 0.24, 0.36, 0.48, 0.6$ (from top to bottom)

how the right-going disturbance wave propagates past the hump. We perform the numerical investigation with our proposed method with triangular partition, as shown in the right panel of Fig. 1. Two distinct mesh sizes $\Delta h = 1/40$ and $\Delta h = 1/160$ are tested. The snapshots of the computed solution at times $t = 0.12, 0.24, 0.36, 0.48$ and 0.6 are shown in Fig. 4. The obtained results clearly show that our method can capture the small perturbation and resolve the complicated features of the studied flow very well.

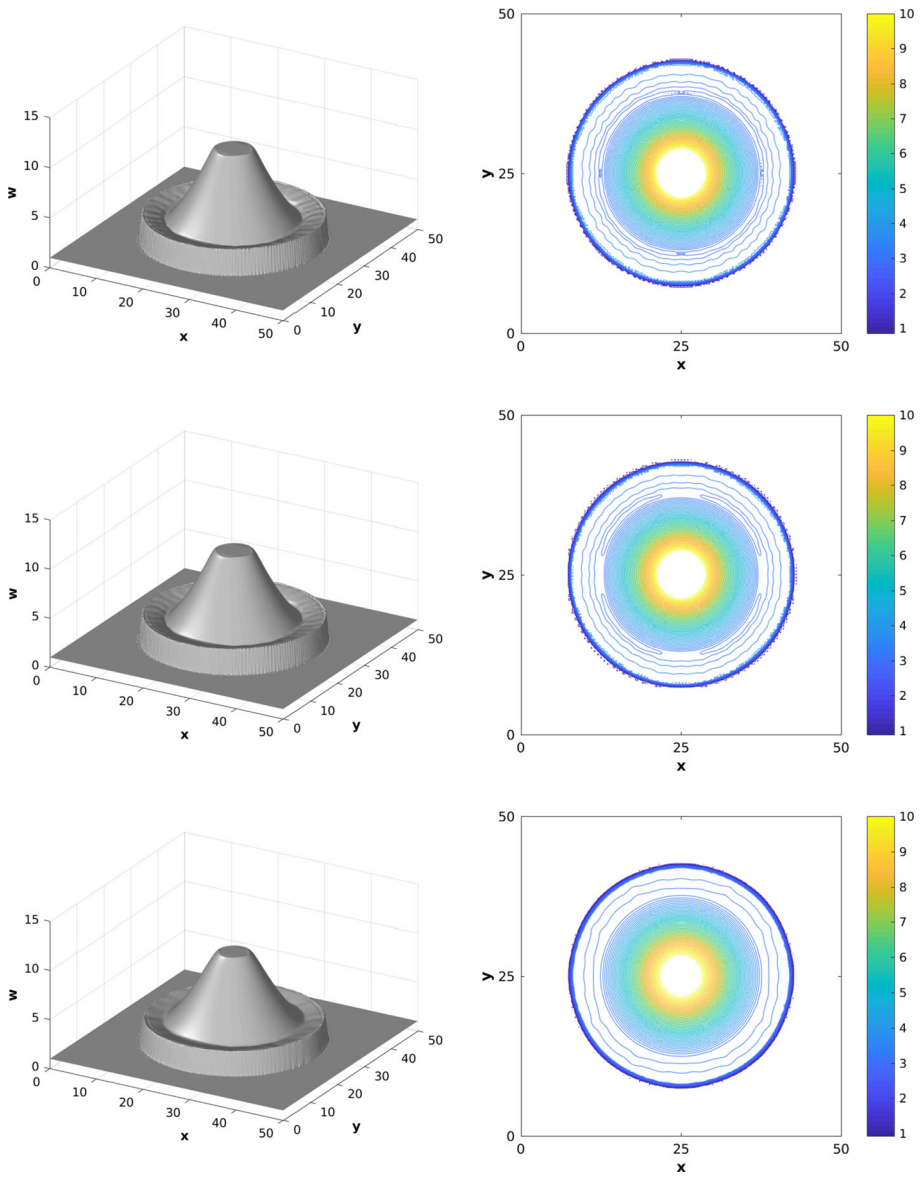

Fig. 5 Example 5: 3D view and contour plot of water surface level w of the circular dam break at output time $t = 0.69$. Top: the results computed by well-balanced DG schemes with HR limiting techniques without remainder correction. Middle: The results computed by well-balanced DG schemes with HR limiting techniques and remainder correction (3.3). Bottom: The results computed by well-balanced DG schemes with HR limiting techniques and remainder correction (3.5), $\gamma = 2$

Example 5 (*Circular dam break problem*) This test case consists of the instantaneous breaking of a cylindrical tank of radius 11 meter centered on a square computational domain $[0, 50] \times [0, 50]$ with a flat bottom topography, initially filled with 10 meter of water at rest. The wave generated by the breaking of the tank propagates into still water with an initial depth of 1 meter. We discretize the domain with the triangular meshes as in the right panel of Fig. 1 and

Δh is taken as 0.5. This classic problem is widely used to test the shock capture capability of numerical schemes [37].

A 3D view and contour lines of the water surface level w at time $t = 0.69$ using different numerical methods are shown in Fig. 5. We can observe that our proposed methods further remove the oscillations in the numerical results, compared with HR limiting techniques only.

5 Conclusion

In this paper, we have developed a high-order accurate and well-balanced DG scheme for solving the Saint–Venant system of shallow water equations on 2D unstructured meshes. Constant subtraction is employed in order to achieve the well-balanced property; while HR limiting with the remainder correction technique is used to further control the possible numerical oscillations. We theoretically show that our proposed DG scheme can retain the well-balanced property while preserving the high order of accuracy. Numerical examples with smooth and discontinuous solutions are provided to demonstrate the effectiveness of our proposed scheme.

References

1. Atkinson, K.E.: An Introduction to Numerical Analysis, 2nd edn. Wiley, New York (1989)
2. Barré de Saint-Venant, A.J.C.: Théorie du mouvement non permanent des eaux, avec application aux crues de rivières et à l'introduction des marées dans leur lit. C.R. Acad. Sci. Paris, 73:237–240 (1871)
3. Behrens, J.: Atmospheric and ocean modeling with an adaptive finite element solver for the shallow-water equations. Appl. Numer. Math. **26**(1–2), 217–226 (1998)
4. Biswas, R., Devine, K.D., Flaherty, J.E.: Parallel, adaptive finite element methods for conservation laws. Appl. Numer. Math. **14**(1–3), 255–283 (1994)
5. Bryson, S., Epshteyn, Y., Kurganov, A., Petrova, G.: Well-balanced positivity preserving central-upwind scheme on triangular grids for the Saint-Venant system. ESAIM Math. Modell. Numer. Anal. **45**(3), 423–446 (2011)
6. Burbeau, A., Sagaut, P., Bruneau, C.-H.: A problem-independent limiter for high-order Runge–Kutta discontinuous Galerkin methods. J. Comput. Phys. **169**(1), 111–150 (2001)
7. Caleffi, V., Valiani, A.: Well-balanced bottom discontinuities treatment for high-order shallow water equations WENO scheme. J. Eng. Mech. **135**(7), 684–696 (2009)
8. Caleffi, V., Valiani, A., Bernini, A.: Fourth-order balanced source term treatment in central WENO schemes for shallow water equations. J. Comput. Phys. **218**(1), 228–245 (2006)
9. Canestrelli, A., Siviglia, A., Dumbser, M., Toro, E.F.: Well-balanced high-order centred schemes for non-conservative hyperbolic systems applications to shallow water equations with fixed and mobile bed. Adv. Water Resour. **32**(6), 834–844 (2009)
10. Chertock, A., Cui, S., Kurganov, A., Wu, T.: Well-balanced positivity preserving central-upwind scheme for the shallow water system with friction terms. Int. J. Numer. Meth. Fluids **78**(6), 355–383 (2015)
11. Cockburn, B., Hou, S., Shu, C.-W.: The Runge–Kutta local projection discontinuous Galerkin finite element method for conservation laws. IV. The multidimensional case. Math. Comput. **54**(190), 545–581 (1990)
12. Cockburn, B., Lin, S.-Y., Shu, C.-W.: TVB Runge–Kutta local projection discontinuous Galerkin finite element method for conservation laws III: one-dimensional systems. J. Comput. Phys. **84**(1), 90–113 (1989)
13. Cockburn, B., Shu, C.-W.: TVB Runge–Kutta local projection discontinuous Galerkin finite element method for conservation laws. II. General framework. Math. Comput. **52**(186), 411–435 (1989)
14. Cockburn, B., Shu, C.-W.: The Runge–Kutta discontinuous Galerkin method for conservation laws V: multidimensional systems. J. Comput. Phys. **141**(2), 199–224 (1998)
15. Harten, A., Engquist, B., Osher, S., Chakravarthy, S.R.: Uniformly high order accurate essentially non-oscillatory schemes. III. In: Upwind and high-resolution schemes, pp. 218–290 (1987)

16. Kurganov, A., Levy, D.: Central-upwind schemes for the Saint–Venant system. ESAIM Math. Modell. Numer. Anal. **36**(3), 397–425 (2002)
17. Kurganov, A., Petrova, G.: A second-order well-balanced positivity preserving central-upwind scheme for the Saint-Venant system. Commun. Math. Sci. **5**(1), 133–160 (2007)
18. LeBlond, P.H.: On tidal propagation in shallow rivers. J. Geophys. Res. Oceans **83**(9), 4717–4721 (1978)
19. LeVeque, R.J.: Balancing source terms and flux gradients in high-resolution Godunov methods: the quasi-steady wave-propagation algorithm. J. Comput. Phys. **146**(1), 346–365 (1998)
20. Li, G., Xing, Y.: Well-balanced finite difference weighted essentially non-oscillatory schemes for the Euler equations with static gravitational fields. Comput. Math. Appl. **75**(6), 2071–2085 (2018)
21. Liu, X., Albright, J., Epshteyn, Y., Kurganov, A.: Well-balanced positivity preserving central-upwind scheme with a novel wet/dry reconstruction on triangular grids for the Saint–Venant system. J. Comput. Phys. **374**, 213–236 (2018)
22. Noelle, S., Xing, Y., Shu, C.-W.: High-order well-balanced schemes. Numerical methods for balance laws. Quaderni di Matematica **24**, 1–66 (2010)
23. Pelinovsky, E., Kharif, C., et al.: Extreme Ocean Waves. Springer, Berlin (2008)
24. Qiu, J., Shu, C.-W.: Runge-Kutta discontinuous Galerkin method using WENO limiters. SIAM J. Sci. Comput. **26**(3), 907–929 (2005)
25. Rhebergen, S., Bokhove, O., van der Vegt, J.J.W.: Discontinuous Galerkin finite element methods for hyperbolic nonconservative partial differential equations. J. Comput. Phys. **227**(3), 1887–1922 (2008)
26. San, O., Kara, K.: High-order accurate spectral difference method for shallow water equations. Int. J. Res. Rev. Appl. Sci. **6**, 41–54 (2011)
27. Shu, C.-W.: TVB uniformly high-order schemes for conservation laws. Math. Comput. **49**(179), 105–121 (1987)
28. Shu, C.-W., Osher, S.: Efficient implementation of essentially non-oscillatory shock-capturing schemes. J. Comput. Phys. **77**(2), 439–471 (1988)
29. Walko, R.L., Avissar, R.: The ocean-land-atmosphere model (OLAM) part I: shallow-water tests. Mon. Weather Rev. **136**(11), 4033–4044 (2008)
30. Wang, Z., Li, G., Delestre, O.: Well-balanced finite difference weighted essentially non-oscillatory schemes for the blood flow model. Int. J. Numer. Meth. Fluids **82**(9), 607–622 (2016)
31. Xing, Y.: Numerical methods for the nonlinear shallow water equations. Handb. Numer. Anal. **18**, 361–384 (2017)
32. Xing, Y., Shu, C.-W.: High order finite difference WENO schemes with the exact conservation property for the shallow water equations. J. Comput. Phys. **208**(1), 206–227 (2005)
33. Xing, Y., Shu, C.-W.: High-order well-balanced finite difference WENO schemes for a class of hyperbolic systems with source terms. J. Sci. Comput. **27**(1–3), 477–494 (2006)
34. Xing, Y., Shu, C.-W.: High order well-balanced finite volume WENO schemes and discontinuous Galerkin methods for a class of hyperbolic systems with source terms. J. Comput. Phys. **214**(2), 567–598 (2006)
35. Xing, Y., Shu, C.-W.: A new approach of high order well-balanced finite volume WENO schemes and discontinuous galerkin methods for a class of hyperbolic systems with source terms. Commun. Comput. Phys. **1**(1), 100–134 (2006)
36. Xing, Y., Shu, C.-W.: A survey of high order schemes for the shallow water equations. J. Math. Study **47**(3), 221–249 (2014)
37. Xing, Y., Zhang, X.: Positivity-preserving well-balanced discontinuous Galerkin methods for the shallow water equations on unstructured triangular meshes. J. Sci. Comput. **57**(1), 19–41 (2013)
38. Xu, Z., Liu, Y., Du, H., Lin, G., Shu, C.-W.: Point-wise hierarchical reconstruction for discontinuous Galerkin and finite volume methods for solving conservation laws. J. Comput. Phys. **230**(17), 6843–6865 (2011)
39. Xu, Z., Liu, Y., Shu, C.-W.: Hierarchical reconstruction for discontinuous Galerkin methods on unstructured grids with a WENO-type linear reconstruction and partial neighboring cells. J. Comput. Phys. **228**, 2194–2212 (2009)
40. Yang, S., Kurganov, A., Liu, Y.: Well-balanced central schemes on overlapping cells with constant subtraction techniques for the Saint–Venant shallow water system. J. Sci. Comput. **63**(3), 678–698 (2015)
41. Zhong, X., Shu, C.-W.: A simple weighted essentially nonoscillatory limiter for Runge–Kutta discontinuous Galerkin methods. J. Comput. Phys. **232**(1), 397–415 (2013)
42. Zhu, J., Qiu, J., Shu, C.-W., Dumbser, M.: Runge–Kutta discontinuous Galerkin method using WENO limiters II: unstructured meshes. J. Comput. Phys. **227**(9), 4330–4353 (2008)
43. Zhu, J., Zhong, X., Shu, C.-W., Qiu, J.: Runge–Kutta discontinuous galerkin method using a new type of WENO limiters on unstructured meshes. J. Comput. Phys. **248**, 200–220 (2013)
44. Zhu, J., Zhong, X., Shu, C.-W., Qiu, J.: Runge–Kutta discontinuous Galerkin method with a simple and compact Hermite WENO limiter. Commun. Comput. Phys. **19**(4), 944–969 (2016)

45. Zhu, J., Zhong, X., Shu, C.-W., Qiu, J.: Runge–Kutta discontinuous Galerkin method with a simple and compact Hermite WENO limiter on unstructured meshes. Commun. Comput. Phys. **21**(3), 623–649 (2017)

Affiliations

Huijing Du[1] · Yingjie Liu[2] · Yuan Liu[3] · Zhiliang Xu[4]

Huijing Du
hdu5@unl.edu

Yingjie Liu
yingjie@math.gatech.edu

Zhiliang Xu
zxu2@nd.edu

1 Department of Mathematics, University of Nebraska-Lincoln, Lincoln, NE 68588, USA

2 School of Mathematics, Georgia Institute of Technology, Atlanta, USA

3 Department of Mathematics, Statistics and Physics, Wichita State University, Wichita, KS 67260, USA

4 Department of Applied and Computational Mathematics and Statistics, University of Notre Dame, Notre Dame, IN 46556, USA